Available online at www.sciencedirect.com
ScienceDirect
Journal of Power Sources 175 (2008) 897–902
JOURNAL OF POWER SOURCES
www.elsevier.com/locate/jpowsour

Short communication

# Electrochemical performance of $In_2O_3$ thin film electrode in lithium cell

Wen-Hsien Ho [a], Ching-Fei Li [b], Han-Chang Liu [b], Shiow-Kang Yen [b,*]

[a] *Taiwan Textile Research Institute, Taipei 23674, Taiwan*
[b] *Department of Materials Engineering, National Chung Hsing University, Taichung 40227, Taiwan*

Received 29 June 2007; received in revised form 2 October 2007; accepted 2 October 2007
Available online 13 October 2007

**Abstract**

Indium oxide ($In_2O_3$) coating on Pt, as an electrode of thin film lithium battery was carried out by using cathodic electrochemical synthesis in $In_2(SO_4)_3$ aqueous solution and subsequently annealing at 400 °C. The coated specimens were characterized by X-ray photoelectron spectroscopy (XPS) for chemical bonding, X-ray diffraction (XRD) for crystal structure, scanning electron microscopy (SEM) for surface morphology, cyclic voltammetry (CV) for electrochemical properties, and charging/discharging test for capacity variations. The $In_2O_3$ coating film composed of nano-sized particles about 40 nm revealing porous structure was used as the anode of a lithium battery. During discharging, six lithium ions were firstly reacted with $In_2O_3$ to form $Li_2O$ and In, and finally the $Li_{4.33}In$ phase was formed between 0.7 and 0.2 V, revealing the finer particles size about 15 nm. The reverse reaction was a removal of $Li^+$ from $Li_{4.33}In$ phase at different oxidative potentials, and the rates of which were controlled by the thermodynamics state initially and diffusion rate finally. Therefore, the total capacity was increased with decreasing current density. However, the cell delivering a stable and reversible capacity of 195 mAh $g^{-1}$ between 1.2 and 0.2 V at 50 μA $cm^{-2}$ may provide a choice of negative electrode applied in thin film lithium batteries.


*Keywords:* Electrolytic deposition; $In_2O_3$ thin film; Lithium battery

## 1. Introduction

Thin film battery markets are anticipated to reach 11 billion dollars by 2012 [1], and a lot of studies were devoted on the research of thin film battery recently [2–8]. In general, the physical vapor deposition (PVD) was usually to use to construct thin film cathode, anode, and electrolyte [9–11]. However, the deposited rate and equipments were too slow and expensive to reduce the production cost of the thin film batteries. Although the sol–gel coating is a potential route, the repeated procedures to coat and pre-sinter in order to achieve the appropriate thickness were unfavorable for manufacturing thin film electrode, especially for the solid-state electrolyte [12]. On the other hand, the electrochemical method was increasingly being used for the preparation of oxide thin films [13], because the coating time was shorter than that sputtering. Straightforwardly the electrolytic coating would be a convenient technology to prepare oxide thin film for lithium battery applications [14–18].

For the safety issue, the development of other anodes has been investigated to replace lithium metal, and the reaction mechanisms with lithium have become a major topic in the area of the energy storage. Among anodes, metal oxides should be paid much attention, especially for $In_2O_3$ due to its applications extensively. Li et al. [19] reported the reaction of $In_2O_3$ prepared by coating mixed-slurries with lithium was similar to the report of $SnO_2$ by Courtney and Dahn [20]. Firstly, the $In_2O_3$ was decomposed into $Li_2O$ and Indium, and secondly three potential plateaus of Li–In appeared ($Li_{0.86}In$, $Li_{1.74}In$, $Li_{2.08}In$, $Li_{2.67}In$). However, Vaughey et al. [21] pointed out five compositions existed in Li–In systems, namely, LiIn, $Li_5In_4$, $Li_3In_2$, $Li_2In$, $Li_{13}In_3$. Also, Zhou et al. [22] revealed the different results instead of the classical alloying reaction between $In_2O_3$ and lithium.

Despite huge specific capacities of $In_2O_3$ with lithium, it seems that the electrochemical performances of material are strongly influenced by its microstructure and composition. As

* Corresponding author. Tel.: +886 4 2852953; fax: +886 4 2857017.
*E-mail address:* skyen@dragon.nuch.edu.tw (S.-K. Yen).

0378-7753/$ – see front matter © 2007 Elsevier B.V. All rights reserved.
doi:10.1016/j.jpowsour.2007.10.020

a result, the electrochemical lithium insertion/extraction properties of both $In_2O_3$ and In should be still further investigated. In this study, $In_2O_3$ films obtained by electrochemical deposition [23] as anodes without any binders and carbon blacks can be helpful to optimize the design of electrodes with improved cycling behavior compared to conventional material. In addition, the electrochemical characterization, structure, composition, and morphology were investigated by cyclic voltammetry (CV), charging/discharging tests, X-ray diffraction (XRD), field-emission scanning electron microscopy (FE-SEM), and X-ray photoelectron spectroscopy (XPS).

## 2. Experimental

### 2.1. Cathodic deposition

In order to obtain $In_2O_3$ coating, the cathodic deposition of $In(OH)_3$ coatings on platinum were first carried out in aerated 0.01 M $In_2(SO_4)_3 \cdot 9H_2O$ aqueous solution for 1200 s, at −1.2 V (Ag/AgCl) by using an EG&G Princeton Applied Research 273A Potentiostat, and subsequently annealed at 400 °C for 1 h. The detailed cathodic reactions during deposition have been reported in the previous paper [23].

### 2.2. XRD and SEM

The crystal structures of the as-deposited and post-annealed films in various heating conditions were analyzed by X-ray diffraction (XRD) in a MAC MO3X-HF diffractometer, with Cu Kα radiation (λ = 1.5418), 2θ in the range 20–43°, at a scanning rate of 1° $min^{-1}$, a voltage of 40 kV, and a current of 30 mA. The surface morphology and cross-sectional view of the deposited specimens were observed by field-emission scanning electron microscopy (JEOL JSM-6700F Japan).

### 2.3. XPS

X-ray photoelectron spectroscopy (XPS) measurements were performed on an ESCA PHI 1600 system with an operating pressure of $1 \times 10^{-8}$ Torr using nonmonochromatized Mg Kα radiation as the excitation source. Peaks were recorded with constant step energy of 0.2 eV, and pass energy of 29.35 eV. To correct possible charge-up of the films by X-ray irradiation, the binding energy was calibrated using C 1s spectrum of hydrocarbon that remained in the XPS analysis chamber as a contaminant.

### 2.4. Electrochemical characterization

For the electrochemical measurements, two-electrode and three-electrode cells were employed with $In_2O_3$ coated specimen, as the working electrode and two lithium thin foils as both the reference and counter electrodes. Prior to fabrication, all $In_2O_3$ coated specimens prepared by annealing at 400 °C for 1 h, were further dried for at least 12 h at 80 °C in a vacuum oven. The electrolyte consisted of 1 M $LiClO_4$ dissolved in

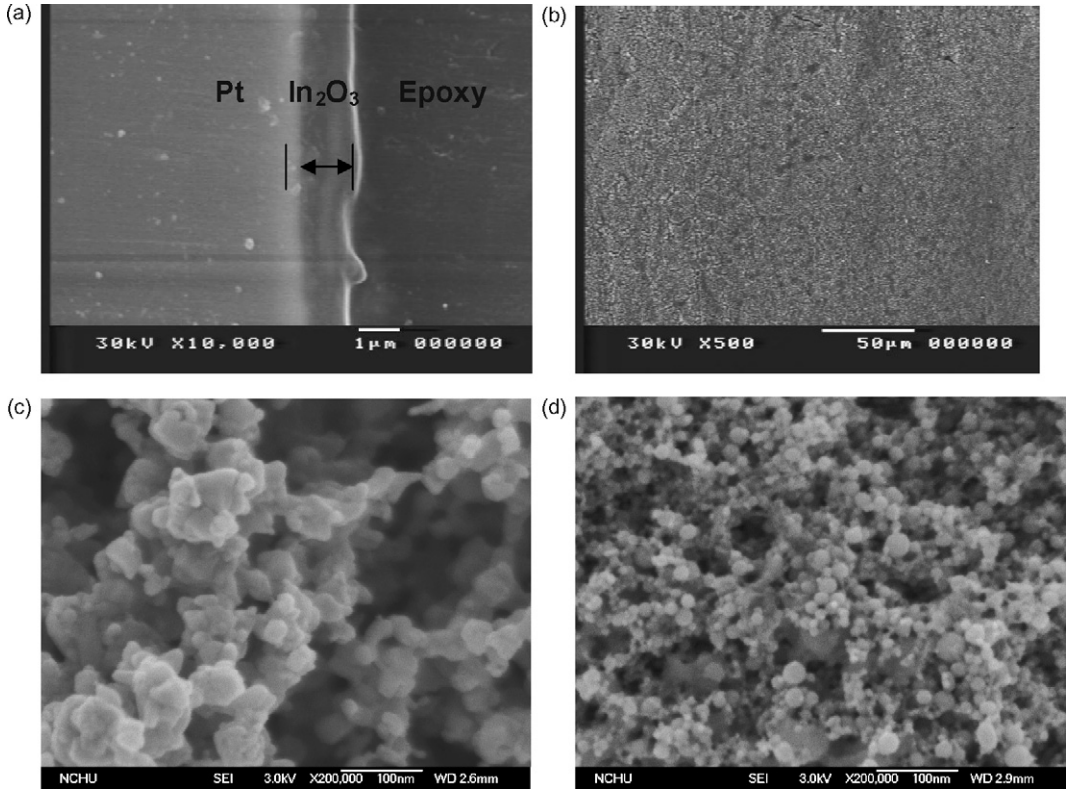


Fig. 1. Cross-sectional view (a), surface morphology of the $In_2O_3$ coated specimen annealed at 400 °C (b) 500× and (c) 200,000×, and after the first discharge (d) 200,000×, respectively.

a nonaqueous solution of propylene carbonate. The cells were assembled in an argon-filled glove box. First cyclic voltammetric (CV) measurement was carried out between 0.2 and 2.2 V (vs. $Li/Li^+$) and the subsequent nine cycles between 0.2 and 1.2 V (vs. $Li/Li^+$) at a scanning rate of 0.5 mV $s^{-1}$ on an EG&G model 273 potentiostat/galvanostat. The charge–discharge measurement was performed at a current density of 50 and 5 μA $cm^{-2}$, respectively, on a Maccor series 2000 battery tester.

## 3. Results and discussion

### 3.1. Surface morphology

The previous paper has indicated that the as-coated film was $In(OH)_3$, transformed into InOOH at 300 °C and finally condensed into $In_2O_3$ [23]. From cross-sectional view, the thickness of electrolytic $In_2O_3$ coated film was about 1.0 μm as shown in Fig. 1(a), and there was a good interface between the coating and the substrate as shown in (b). Particles tended to agglomerate to form porous layer and exhibited a uniform distribution in terms of particle size about 20–50 nm, as shown in Fig. 1(c).

### 3.2. Electrochemical properties

The first CV diagram (Fig. 2) of the $In_2O_3$ cathode, which was recorded at a scanning rate of 0.5 mV $s^{-1}$ between 2.2 and 0.2 V, shows three current peaks at 1.2, 0.8, and 0.48 V during discharging, and the other three peaks at 0.65, 1.05, and 1.70 V during charging. Three corresponding discharging plateaus were also found in the constant current chronopotentiometry, as shown in Fig. 3. For the first reaction, six lithium ions with oxygen bound to In, as shown in Fig. 3 plateaus I and II. In other words,

$$6Li^+ + 6e^- + In_2O_3 \rightarrow 3Li_2O + 2In \quad (1)$$

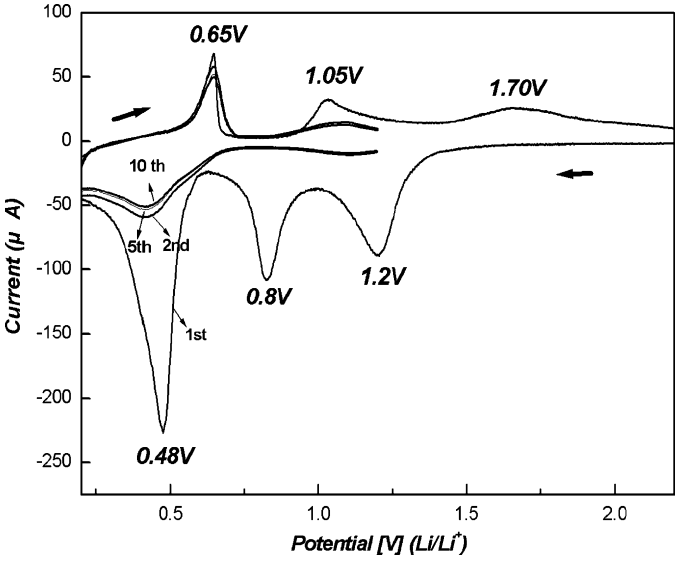


Fig. 2. The first cyclic voltammogram of the $In_2O_3$ film annealed at 400 °C in liquid electrolyte cells, at a scanning rate of 0.5 mV $s^{-1}$ between 2.2 and 0.2 V ($Li/Li^+$), and the subsequent nine cycles between 1.2 and 0.2 V ($Li/Li^+$).

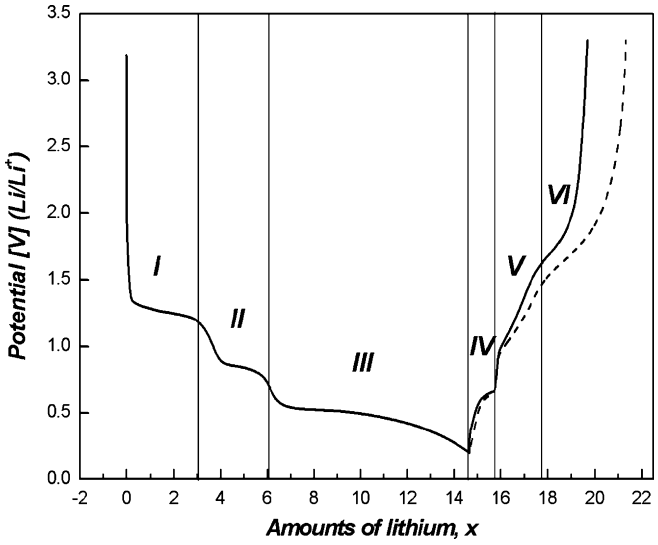


Fig. 3. The first charge/discharge curve of the $In_2O_3$ film annealed at 400 °C in liquid electrolyte cells between 3.23 and 0.2 V ($Li/Li^+$) at a charge/discharge rate of 50 μA $cm^{-2}$ (solid line) and 5 μA $cm^{-2}$ (dash line), respectively.

occurred and accomplished at the end of 0.7 V. This argument was also supported by XRD results, which revealed the diffraction peak of In metal as shown in Fig. 4(a). Besides, the particles were pulverized into the fine size (10–15 nm), as shown in Fig. 1(d). However, the peaks of $Li_2O$ were never found in XRD data. The amorphous structure of $Li_2O$ should be supposed, and the similar results were also found in $SnO_2$ and CoO [24,25]. This result was consistent with XPS spectra. The binding energy of In $3d_{5/2}$ is at 444.5 eV as shown in Fig. 5(a), indicating the $In^{3+}$ bonding in $In_2O_3$. When discharging to 0.7 V, the electron binding energy of In $3d_{5/2}$ shifts slightly to lower energy, meaning a valence state change of In [26]. In the meanwhile, the binding energy peak of lithium 1s appears at about 55.5 eV as shown in Fig. 5(b), which can be assigned to amorphous $Li_2O$. Following plateaus I and II, it was the insertion of 8.66 lithium ions into indium, as shown in Fig. 3 plateau III. The alloying of indium with lithium,

$$zLi^+ + ze^- + In \rightarrow Li_zIn \quad (0 < z \leqq 4.33) \quad (2)$$

This reaction proceeded between 0.7 and 0.2 V. It was also supported by the XRD results, which revealed the diffraction peaks of $Li_zIn$ and the disappearance of In, as shown in Fig. 4(b). Similarly, other reports under dynamic electrochemical conditions [27,28] do not show the individual-phase differentiation so clearly. As a result, the total reaction combined with the reactions (1) and (2) on the first reduction was as follows:

$$14.66Li^+ + 14.66e^- + In_2O_3 \rightarrow 3Li_2O + 2Li_{4.33}In \quad (3)$$

The total specific capacity was 1415 mAh $g^{-1}$ on the basis of the weight gain (0.44 mg $In_2O_3$) to the total charge (2.24 C). On the other hand, the three oxidation peaks located around 0.65, 1.05, and 1.70 V were found in the cyclic voltammogram (Fig. 2). However, only five $Li^+$ ion could be removed from $8.66Li^+$ in $Li_{4.33}In$ after charging to 3.23 V, as the solid line curve shown in Fig. 3 plateaus IV, V, and VI. The final phase after charged was

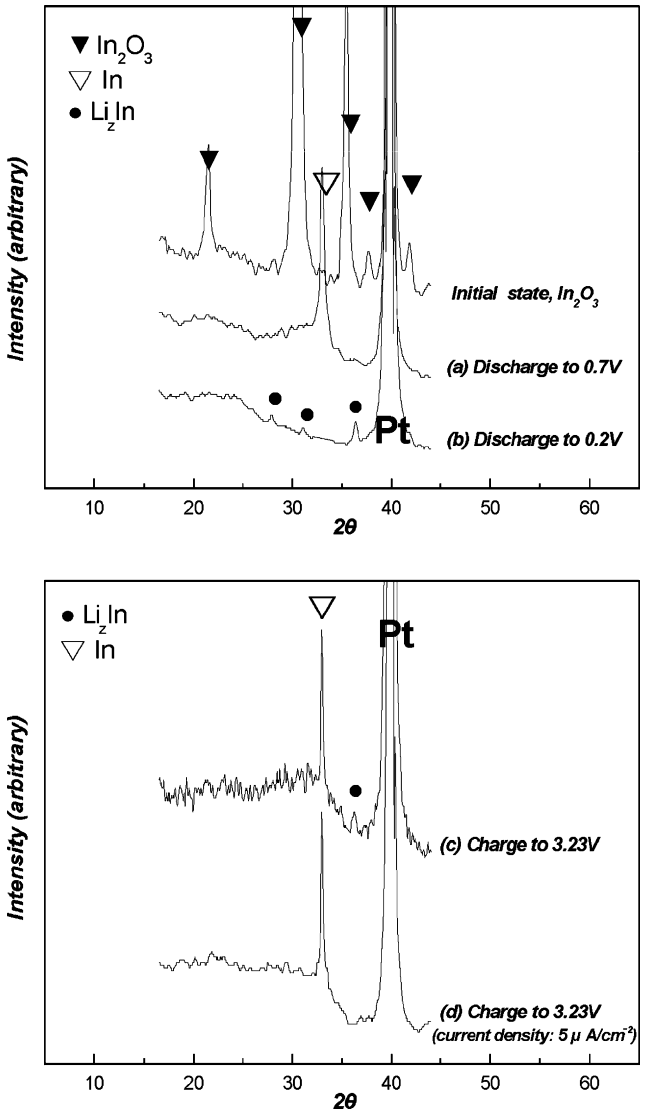


Fig. 4. XRD diagrams of the $In_2O_3$ film annealed at 400 °C before discharging, after discharging to (a) 0.7 V and (b) 0.2 V, subsequently charging to (c) 3.23 V at a current density of 50 μA $cm^{-2}$, and another charging from 0.2 V to (d) 3.23 V at a lower current density of 5 μA $cm^{-2}$. ▼, □, and ● are the symbols of $In_2O_3$, In, and $Li_zIn$ phases, respectively.

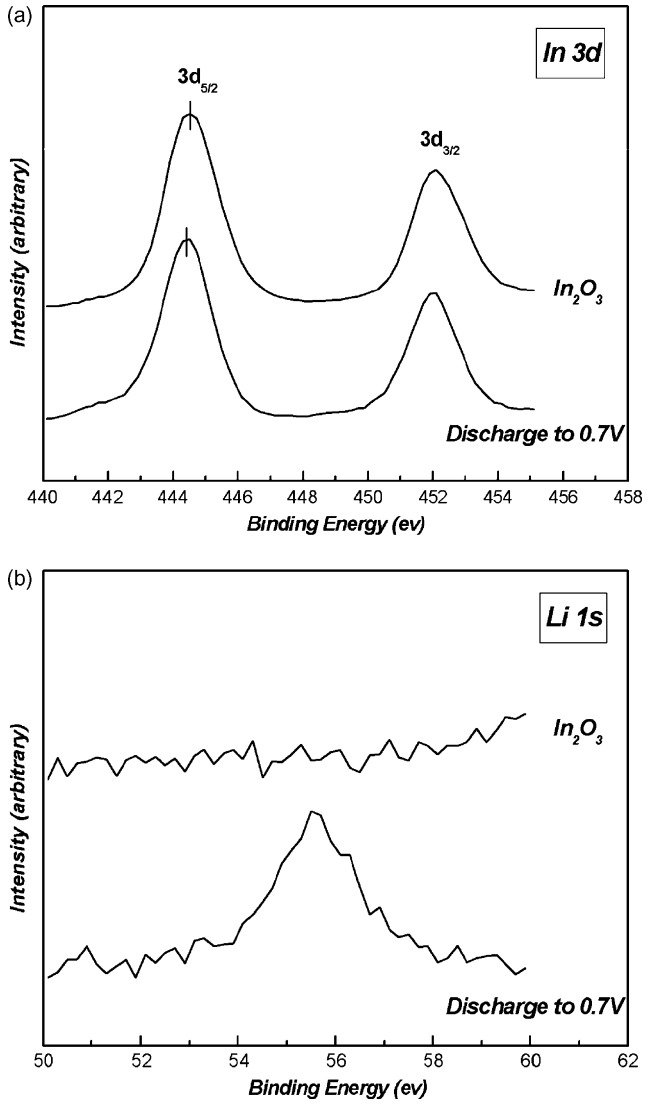


Fig. 5. XPS spectra of the $In_2O_3$ film electrode annealed at 400 °C before discharging (a), and after discharging to 0.7 V (b).

found to be In and $Li_{4.33}In$, as shown in Fig. 4(c). Obviously, the three oxidative peaks located 0.65, 1.05, and 1.70 V was not attributed to the reverse reactions of (2) and (1), respectively, but only to (2). The remained $Li_{4.33}In$ means that the reverse reaction of (2) was not completed. Only 57.7% of $Li_{4.33}In$ was reversed into In, according to the ratio of 5–8.66 lithium ions. If 57.7% of $Li_zIn$ was accounted into the reverse reaction of (2), the plateaus IV, V, and VI in Fig. 3, which are corresponding to the oxidative peaks located at 0.65, 1.05, and 1.70 V, could be presented by the following reactions, respectively

$$Li_{4.33}In \rightarrow Li_{3.5}In + 0.83Li^+ + 0.83e^- \quad (4)$$

$$Li_{3.5}In \rightarrow Li_{1.75}In + 1.75Li^+ + 1.75e^- \quad (5)$$

$$Li_{1.75}In \rightarrow 1.75Li^+ + 1.75e^- + In \quad (6)$$

Reactions (4)–(6) can be ascribed to the reversible reaction among lithium–indium alloys of different stoichiometry. In order to understand the relationship between "plateau potential" and $z$ in $Li_zIn$ alloy, the phase diagrams [29] were very useful tools for presenting and understanding thermodynamic information in opposition to calculation by the use of thermodynamic principles [28]. $Li_{3.5}In$ in reaction (4) may be composed of $Li_4In$ and $Li_3In$, and $Li_{1.75}In$ in reaction (5) of $Li_2In$ and LiIn [23]. When the reaction rate in (4) is controlled by the diffusion rate or thermodynamics state in the inner $Li_{4.33}In$, reaction (5) subsequently proceeded for keeping constant current density, and so did reaction (6) finally. This argument is supported by the charging measurement carried out at a lower current density of 5 μA $cm^{-2}$, as the dash line curve shown in Fig. 3. The 76% of $Li_{4.33}In$ was accounted into the reverse reaction of (2). Obviously, the reversibility and capacity of reactions (5) and (6) (plateaus V and VI) was increased with decreasing current density. This means that the diffusion rate of $Li^+$ may control the reaction rates of (5) and (6). When the applied current density

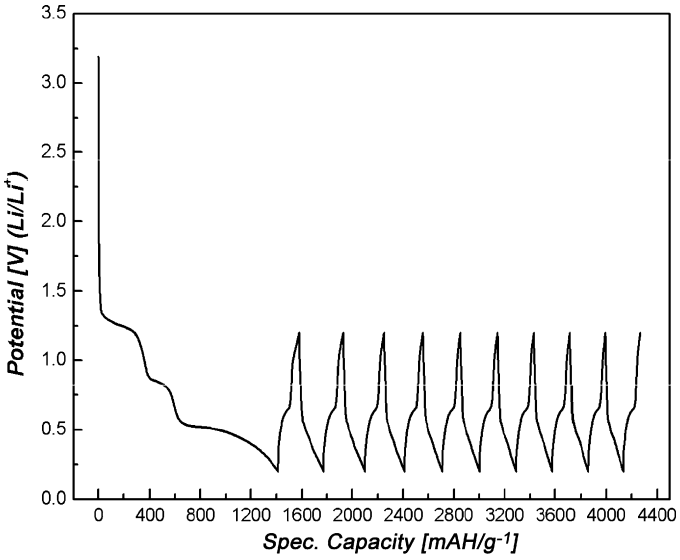


Fig. 6. The subsequent charge/discharge curves of the $In_2O_3$ film annealed at 400 °C in liquid electrolyte cells, at a charge/discharge rate of 50 μA cm$^{-2}$ between 1.2 and 0.2 V (Li/Li$^+$).

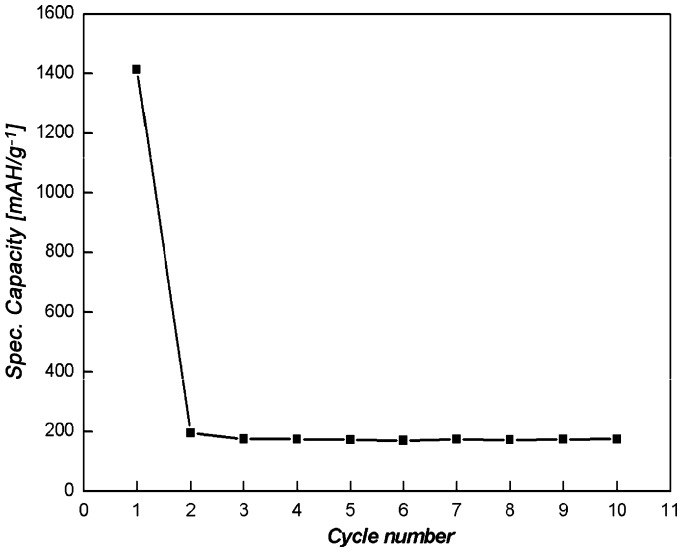


Fig. 7. The evolution of discharge capacity vs. the cycle number for the $In_2O_3$ film annealed at 400 °C in liquid electrolyte cells at a charge/discharge rate of 50 μA cm$^{-2}$ between 0.2 and 1.2 V (Li/Li$^+$).

is decreased to the diffusion rate of $Li^+$, the electrochemical reaction of (5) and (6) is approaching to be totally reversible. Compared with Fig. 4(c), much less $Li_{4.33}In$ was retained, as shown in Fig. 4(d). However, reaction (4) (plateau IV) is independent of charging current density, but dependent on potential. It is consistent with Nernstian equation, or thermodynamic control. In other words, the diffusion rate of $Li^+$ in $Li_{4.3}In$ is much faster than that in $Li_{3.5}In$ and $Li_{1.75}In$. This is also the factor that resulted in revealing one plateau (plateau III in Fig. 3) on the discharge process, whereas three plateaus (plateaus IV, V, and VI) on the charge process. In spite of the increasing removal amounts of lithium with charging to higher voltage of 3.23 V, the reversibility was decreased seriously due to grain growth of In from 14 to 40 nm calculated by Fig. 4(a) and (c) according to Scherrer–Bragg equation

$$l\,(\mathrm{nm}) = \frac{0.9\lambda}{B\cos\theta}$$

where $B$ is the full-width at half-maximum (FWHM) of the diffraction peak, λ the X-ray wavelength (nm) and $\theta$ is the diffracting angle. As a result, the charging–discharging ranges should be controlled between 0.2 and 1.2 V in this study. The present results were different from the report by Fu et al. [22]. They indicated that the first discharging reaction was $In_2O_3 + 10Li^+ + 10e^- \rightarrow 2Li_2In + 3Li_2O$, and the subsequent charging was partially reversible due to the decomposition of $Li_2O$ driven by nano-sized metal In (<6 nm). Revealing the different reactions of $In_2O_3$ with lithium may be resulted from different particle size of $In_2O_3$ and/or In which were prepared by different methods. In this study, this cell prepared by electrolytic deposition revealing the strong adhesion of active materials with the substrate (Fig. 1(b)) delivered a stable capacity 195 mAh g$^{-1}$, as shown in Fig. 6. Because the first discharge took a large ratio of time, only 10 cycles are shown here. No obvious decreasing of capacity was found after 50 cycles. Also, the morphology and structure of electrode after tests were similar to those of the first discharging one at a fixed current density. The subsequent nine CV diagrams and capacities versus increasing cycle number were also shown in Figs. 2 and 7, respectively. This means that reactions (4) and (5) are reversible for the 57.7% of $Li_{4.33}In$ in lithia matrix at current density of 50 μA cm$^{-2}$ (0.1 C).

## 4. Summary and conclusion

The electrolytic method has been successfully used to fabricate the porous $In_2O_3$ thin films in a naturally aerated 0.01 M $In_2(SO_4)_3$ solution, for lithium ion battery electrodes. The electrochemistry of $In_2O_3$ with lithium ion was expressed as follows:

$$6Li^+ + 6e^- + In_2O_3 \rightarrow 3Li_2O + 2In \quad (1)$$

and

$$4.33Li^+ + 4.33e^- + In \rightarrow Li_{4.33}In \quad (2)$$

for discharging. Although the reverse reaction of (1) was not found in charging, the 57.7% of $Li_{4.33}In$ was accounted into the reverse reaction of (2) during charging. The details of reverse reaction (2) contained

$$Li_{4.33}In \rightarrow Li_{3.5}In(Li_4In + Li_3In) + 0.83Li^+ + 0.83e^- \quad (4)$$

$$Li_{3.5}In \rightarrow Li_{1.75}(Li_2In + LiIn) + 1.75Li^+ + 1.75e^- \quad (5)$$

and

$$Li_{1.75}In \rightarrow 1.75Li^+ + 1.75e^- + In \quad (6)$$

The reaction state of (4) was controlled by thermodynamics (Nernstian equation) and the reaction rates of (5) and (6) were controlled by the diffusion. Also, the Li–$In_2O_3$ cell delivering a stable capacity of 195 mAh g$^{-1}$ in the potential range between 1.2 and 0.2 V at 50 μA cm$^{-2}$ may provide another choice of negative electrode applied in thin film lithium batteries.

## Acknowledgments

The authors are grateful for the support of this research by the Department of Industrial Technology, Ministry of Economic Affairs, Republic of China under contract Nos. 96-EC-17-A-99-R1-0641 and 96-EC-17-A-11-R7-0330.

## References

[1] Nanotechnology and Thin Film Lithium and Lithium Ion Battery Market Opportunities, Market Forecasts, and Market Strategies 2006–2012, WinterGreen Research, Inc., Lexington, MA, 2006.
[2] N.J. Dudney, Mater. Sci. Eng. B 116 (2005) 245.
[3] N. Kuwata, R. Kumar, K. Toribami, T. Suzuki, T. Hattori, J. Kawamura, Solid State Ionics 177 (2006) 2827.
[4] Y. Iriyama, C. Yada, T. Abe, Z. Ogumi, K. Kikuchi, Electrochem. Commun. 8 (2006) 1287.
[5] Y.H. Rho, K. Kanamura, J. Power Sources 158 (2006) 1436.
[6] J. Schwenzel, V. Thangadurai, W. Weppner, J. Power Sources 154 (2006) 232.
[7] W.Y. Liu, Z.W. Fu, Q.Z. Qin, Thin Solid Films 515 (2007) 4045.
[8] H. Kim, R.C.Y. Auyeung, A. Pique, J. Power Sources 165 (2007) 413.
[9] Y.J. Park, K.S. Park, J.G. Kim, M.K. Kim, H.G. Kim, H.T. Chung, J. Power Sources 88 (2000) 250.
[10] M. Baba, N. Kumagai, N. Fujita, K. Ohta, K. Nishidate, S. Komaba, J. Power Sources 97–98 (2001) 798.
[11] E. Jeong, C. Hong, Y. Tak, S.C. Nam, S. Cho, J. Power Sources 159 (2006) 223.
[12] C.H. Park, M. Park, S.I. Yoo, S.K. Joo, J. Power Sources 158 (2006) 1442.
[13] I. Zhitomirsky, Adv. Colloid Interf. Sci. 97 (2002) 279.
[14] W.H. Ho, S.K. Yen, J. Electrochem. Soc. A506 (2005) 152.
[15] W.H. Ho, S.K. Yen, Electrochem. Solid-State Lett. C134 (2005) 8.
[16] H.C. Liu, S.K. Yen, J. Power Sources 159 (2006) 245.
[17] W.H. Ho, S.K. Yen, Surf. Coat. Technol. 201 (2007) 7100.
[18] H.C. Liu, S.K. Yen, J. Power Sources 166 (2007) 478.
[19] H. Li, X. Huang, L. Chen, Solid State Ionics 123 (1999) 189.
[20] I.A. Courtney, J.R. Dahn, J. Electrochem. Soc. 144 (1997) 2045.
[21] J.T. Vaughey, C.S. Johnson, A.J. Kropf, R. Benedek, M.M. Thackeray, H. Tostmann, T. Sarakonsri, S. Hackney, L. Fransson, K. Edstrom, J.O. Thomas, J. Power Sources 97–98 (2001) 194.
[22] Y. Zhou, H. Zhang, M. Xue, C. Wu, X. Wu, Z. Fu, J. Power Sources 162 (2006) 1373.
[23] W.H. Ho, S.K. Yen, Thin Solid Films 498 (2006) 80.
[24] T. Brousse, R. Retoux, U. Herterich, D.M. Schleich, J. Electrochem. Soc. 145 (1998) 1.
[25] P. Poizot, S. Laruelle, S. Grugeon, L. Dupont, J.M. Tarascon, Nature 407 (2000) 496.
[26] J.F. Moulder, W.F. Stickle, P.E. Sobol, K.D. Bomben, Handbook of X-Ray Photoelectron Spectroscopy, Perkin-Elmer Corporation, Eden Prairie, MN, 1992.
[27] I.A. Courtney, J.R. Dahn, J. Electrochem. Soc. 144 (1997) 2943.
[28] R.A. Huggins, J. Power Sources 81–82 (1999) 13.
[29] W.A. Alexander, L.D. Calvert, R.H. Gamble, K. Schinzel, Can. J. Chem. 54 (1976) 1052.